Journal of
Ceramic Science
and Technology

J. Ceram. Sci. Technol., **14** [2] 81-88 (2023)
DOI: 10.4416/JCST2023-00008
available online at: http://www.ceramic-science.com

Enhancing the Mechanical Properties of (Hf-Ta-Ti-Zr-Nb)C High-Entropy Carbides Using a Multi-Step Spark Plasma Sintering Process

J. Song[1], J. Seok[1, 2], S.-Y. Kim[1, 2], J. Han[1], H. Kim*[1]

[1]Korea Institute of Industrial Technology, 156, Gaetbeol-ro, Yeonsu-gu, Incheon, Republic of Korea
[2]Department of Materials Science and Engineering, INHA UNIVERSITY, 100 Inha-ro, Michuhol-gu, Incheon 22212, Republic of Korea

received May 11, 2023; received in revised form August 3, 2023; accepted August 12, 2023

Abstract

In this study, we investigate a multi-step spark plasma sintering (SPS) process for (Hf-Ta-Ti-Zr-Nb)C high-entropy carbides to produce dense, homogeneous carbide materials with superior mechanical properties. The process consists of compacting a high-entropy carbide powder mixture into a green body and sintering it under high-temperature plasma generated by a pulsed direct current voltage. The single-step of SPS achieves partial densification and solidification of the carbide material, while the multi-step process involves enhancing the microstructure and mechanical properties of the final product. Our results demonstrate that the multi-step SPS process effectively produces high-entropy carbides that are denser and harder, with improved mechanical properties. This establishes the multi-step SPS process as a promising technique for the fabrication of advanced carbide materials.

Keywords: High-entropy carbide, multi-step spark plasma sintering, mechanical properties

I. Introduction

The concept of high-entropy alloys (HEAs) was initially proposed in 2004 [1,2]. HEAs typically consist of at least five elements at equimolar (or near-equal) ratios, according to the definition of high entropy, with minimum entropy $S \geq 1.5R$ ($S = R\ln N$) [3,4]. Due to the high configurational entropy, HEAs usually exhibit single-phase structures with simple lattice geometries. The negative TS term in Gibb's free energy equation ($G = H - TS$) becomes more dominant at high temperatures, leading to greater thermodynamic stability for high-entropy phases [5–7]. Furthermore, HEAs generally display superior mechanical and physical properties such as high strength, hardness, outstanding high-temperature strength, structural stability, as well as excellent corrosion and oxidation resistance [8–10].

The entropy-stabilization concept has also been applied to prepare high-entropy ceramics (e.g. oxides, carbides, borides, and silicides) [11–12]. High-entropy carbides (HECs) are multi-component materials composed of five or more different carbides in equiatomic or near-equiatomic distributions [13]. These materials possess high configurational entropy, which favors the formation of high-entropy phases such as solid solutions while minimizing other phases such as intermetallics [14–16]. The resulting single-phase crystal structures exhibit severe lattice distortion and sluggish diffusion effects, leading to enhanced mechanical properties [17]. Additionally, HECs possess mixed bonds characterized by a combination of covalent, ionic, and metallic bonds, which results in an intriguing set of properties such as high melting points, and excellent thermal and electrical conductivity [18–21]. Due to these characteristics, HECs are suitable for applications requiring exceptional mechanical properties and stability at high temperatures, such as aerospace components, drill bits, and cutting tools in mining and industry [22–24].

Fabricating bulk HECs requires either high temperatures or extended processing times due to the strong bonds, low self-diffusion coefficients, and high melting points of ceramics [25–26]. Conventional sintering processes struggle to produce high-density bulk HECs, making alternative methods such as spark plasma sintering (SPS), hot pressing (HP), or hot isostatic pressing (HIP) more suitable [12, 20, 27]. Castle *et al.* was the first to report the synthesis of high-entropy carbides from the transition-metal carbides of HfC, TaC, ZrC, NbC, and TiC using a two-step SPS method involving holding at 1 800 °C under 14 to 40 MPa for ten minutes and at 2 300 °C under 16 MPa for two minutes to form high-entropy (Hf-Ta-Zr-Ti)C and (Hf-Ta-Zr-Nb)C ultra-high-temperature carbides [28]. Other researchers have also reported the fabrication of bulk HECs with SPS, HP, and HIP methods at various temperatures and pressures [29–30].

However, the multi-step SPS of high-entropy carbides has its limitations, such as the potential formation of secondary phases due to the use of rapid heating and cooling rates, which can degrade the material's mechanical properties and limit industrial applications. To address this issue, a multi-step SPS process can be employed, involving a series of heating and cooling steps to control the material's

* Corresponding author: hyoseop1231@kitech.re.kr

microstructure more effectively and minimize the formation of secondary phases.

In this study, we developed a multi-step SPS process to fabricate dense and homogeneous (Hf-Ta-Ti-Zr-Nb)C high-entropy carbides with improved mechanical properties. By adjusting the sintering temperature and uniaxial pressure, we aimed to maximize the density and hardness of the resulting HECs. We also compared single-step and multi-step sintering processes, emphasizing the advantages of the multi-step approach. Our findings show that the multi-step SPS process effectively produces high-entropy carbides with superior properties, making it a promising technique for advanced carbide materials for use in high-performance applications.

II. Experimental Procedure

Five commercial carbides, in this case HfC (99.5 %, 1 μm), TaC (99.5 %, 1 μm), TiC (99.5 %, 2–3 μm), ZrC (99.5 %, 1 μm), and NbC (99 %, < 3 μm), were employed as starting materials in the present study. Their chemical compositions are presented in Fig. 1. In order to determine the optimal powder fabrication conditions suitable for the sintering process, carbide powders with different particle sizes and shapes were subjected to high-energy ball milling. The effects of the refinement and homogeneity of the mixtures were observed. The cylindrical cemented carbide jar used in the ball mill had a diameter of 74 mm and a length of 60 mm. The equipment was designed to cool down the external surface of the jar using cooling water. The cover of the jar was equipped with an O-ring to keep the internal pressure constant by preventing atmospheric gases from leaking. Cemented carbide balls with a diameter of 5.0 mm were used in an atmospheric environment, and the weight ratio of the balls to the powder was set to 10:1. During the refinement process, the ball-milling rotation speed was fixed at 600 rpm, while the ball-milling time was varied by 60 minutes. In addition, circulation cooling was conducted using cooling water to prevent the powder particles from adhering to each other due to the frictional heat generated from the high rotation speed of the ball mill while facilitating fragmentation over the entire course of the refinement process. Four grams of the obtained (Hf-Ta-Ti-Zr-Nb)C high-entropy carbide powder were put into a graphite mold with an inner diameter of 10 mm and an outer diameter of 30 mm, with a subsequent SPS process used to obtain a bulk sample. Before the sintering process, a thin layer of boron nitride spray was applied as a release agent to provide lubrication between the inner surface of the graphite mold and the powder particles. Thermal imaging cameras were also equipped to measure the sintering temperature accurately. During the SPS process, the sintering pressures were fixed at 50, 55, and 60 MPa, and the sintering temperatures were set to 1 700, 1 800, 1 900°C, and 2 000 °C. Subsequently, changes in the microstructure, phase, and mechanical properties of the sintered carbides obtained by means of the SPS process were observed using an X-ray diffractometer (XRD, BRUKER AXS, D8ADVANCE) and a field emission scanning electron microscope (FE-SEM, Hitachi). Their mechanical properties were further characterized based on measurement of the Archimedes density (Alfa Mirage, SD-120L) and Vickers hardness (Wilson VH3300). Indentation and crack dimensions were measured, and the corresponding fracture toughness was calculated and analyzed. Based on the results, the applicability of these materials as a candidate for super-hard tool materials was verified.

(Hf-Ti-Ta-Zr-Nb)C High-entropy carbide milled powders

%	HfC	TiC	TaC	ZrC	NbC	Composition
at.%	1	1	1	1	1	(Hf-Ti-Ta-Zr-Nb)C
wt.%	29.2	9.2	29.6	15.9	16.1	

⇩

Sintering (Spark Plasma Sintering, Sample size : ⌀ 10 × 5mm)

⇩

Characteristics (Microstructures, Mechanical property)

Fig. 1: Flowchart showing the process designed for spark plasma sintering of high-entropy carbide powders.

III. Results and Discussion

A schematic diagram of the SPS bulk fabrication process for (Hf-Ta-Ti-Zr-Nb)C high-entropy carbides via spark plasma sintering is presented in Fig. 1. The initial step involves the preparation of HfC, TiC, TaC, ZrC, and NbC carbide raw powders from the five constituent elements. These carbide powders are subsequently subjected to high-energy ball milling. The die is then positioned within the SPS apparatus, and the sintering process commences. The resulting SPS samples have a diameter of 10 mm and a height of 5 mm.

Fig. 2 presents the multi-step heat treatment curve for (Hf-Ta-Ti-Zr-Nb)C high-entropy carbide powders milled for 60 min using the SPS process. A significant challenge associated with single-step SPS of high-entropy carbides is the potential introduction of non-uniformity in both microstructure and properties of the final bulk, due to suboptimal sintering conditions for individual carbides within the high-entropy carbide system. Consequently, some carbides may undergo more complete sintering than others, resulting in a non-uniform distribution of carbide phases and compromised material properties. To address this issue, multiple steps of spark plasma sintering may be required to ensure complete sintering of each carbide and uniformity in microstructure throughout the material. To effectively sinter the challenging high-entropy carbide powder, a heat treatment was performed, as depicted in Fig. 2. Sample A represents the heat treatment curve obtained via single-step sintering, while Samples B, C, and D correspond to heat treatment conditions with varying hold times at a final sintering temperature of 2 000 °C following a ten-minute hold at 1 800 °C. Song *et al.* [31] reported on single-step sintering of high-entropy carbide, involving sintering at temperatures ranging from 1 700 °C to 2 000 °C for a ten-minute holding time. Their results indicated that multi-carbide phases tended to coalesce into

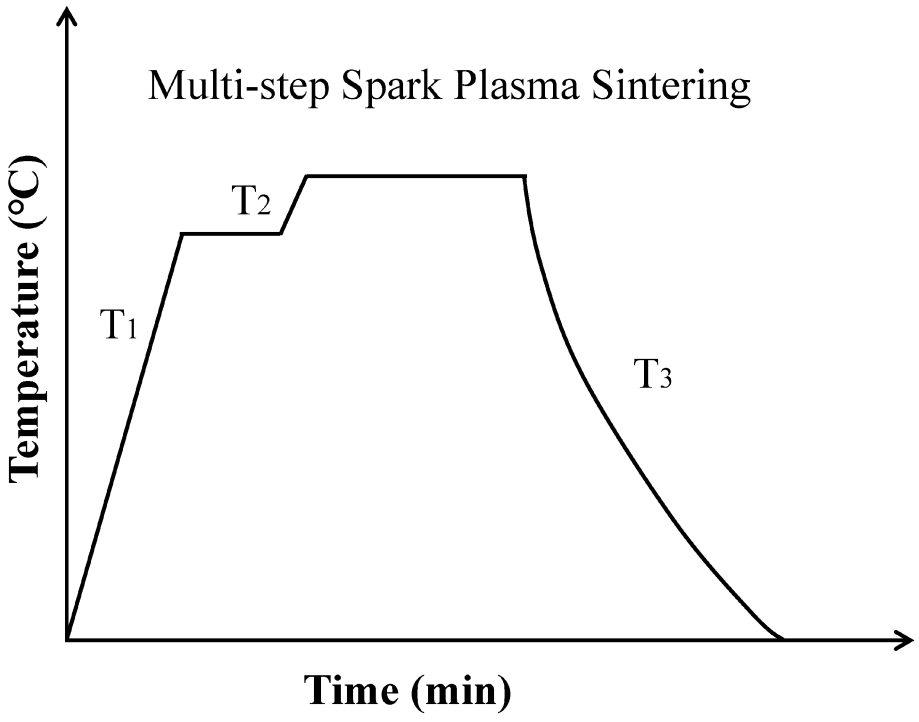

T1 : 1400 °C (100 K/min) → 1500 °C (50 K/min) → 1800 °C (20 K/min)
T2 : 2000 °C (20 K/min)
T3 : 100 K/min of cooling rate

Sample Name	1st Step			2nd Step		
	Temperature (°C)	Pressure (MPa)	Holding Time (min)	Temperature (°C)	Pressure (MPa)	Holding Time (min)
A	2000	50	10	-	-	-
B	1800	60	10	2000	60	1
C	1800	60	10	2000	60	2
D	1800	60	10	2000	60	5

Fig. 2: Heat treatment conditions for multi-step spark plasma sintering.

a single FCC phase as the sintering temperature progressively increased to 2 000 °C. The peak was observed to merge with the FCC phase at 1 800 °C, as revealed in their study.

Fig. 3 shows the X-ray diffraction patterns of (Hf-Ta-Ti-Zr-Nb)C high-entropy carbide samples produced using both single-step and multi-step sintering processes at 2 000 °C for pressure and holding times. After sintering, all peaks relating to individual carbide phases have disappeared, leaving one set of a new cubic phase regardless of the process used. This phase has the NaCl (Fm-3 m) rock-salt structure and shows the formation of a unique solid-solution HEC phase [32]. Peaks corresponding to HfO_2 and ZrO_2 oxides were also observed. This suggests that oxygen introduced during milling in an atmospheric environment caused the high-entropy carbide powder to recrystallize into two phases. These phases were an FCC solid solution phase and an oxide phase. This is considered to be the reason why HfO_2 and ZrO_2 oxide phases were detected in the (Hf-Ta-Ti-Zr-Nb)C composition [33]. HEC sintering was possible at 1 700 °C, but individual carbides were observed in some microstructures. To investigate the difference between single-step and multi-step sintering methods, various sintering temperatures, pressures, and holding times were applied to observe the HEC microstructure. The results are shown in Fig. 4.

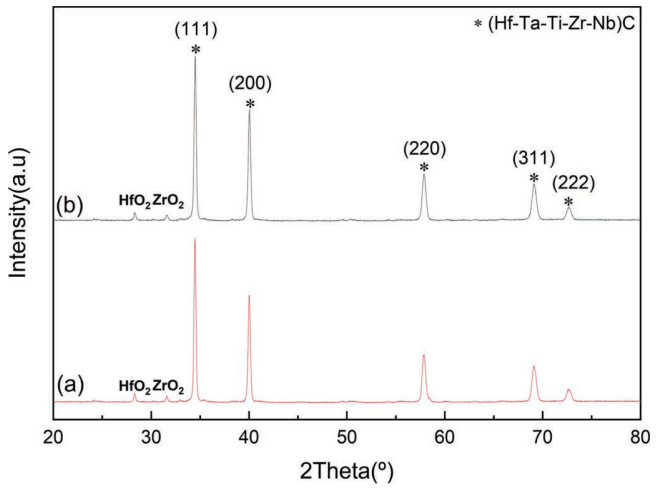

Fig. 3: XRD patterns of (Hf-Ta-Ti-Zr-Nb)C sintered bulk as a function of the SPS method. (a) 2 000 °C, 50 MPa, 10 min (single-step), and (b) 2 000 °C, 60 MPa, 1 min (multi-step).

Fig. 4(a) shows the presence of some pores and individual carbide elements due to the relatively low temperature. However, Figs. 4(b) and (c), which show samples sintered at 2 000 °C using single-step and multi-step methods, respectively, reveal microstructures with significantly reduced porosity. The grain sizes were measured to be approximately 2 – 4 μm and 1 – 3 μm, respectively. This is thought to be closely related to the holding time of SPS. The longer holding time of the sintered body in Fig. 5(b) compared to 5(c) is believed to have resulted in grain growth [34].

Fig. 5 presents the temperature-dependent changes in the relative density and Vickers hardness of HEC samples produced using the single-step SPS technique. As the sintering temperature increases, the density rises gradually from approximately 96 % to nearly 97.8 %. In parallel, Vickers hardness displays an increasing trend from 1 700 HV to a peak of 1 810 HV, followed by a slight reduction at the maximum sintering temperature of 2 000 °C. Despite the emergence of an FCC phase at 1 700 °C, attaining the desired mechanical properties of the carbide is essential for its practical implementation in tools, as mentioned in the previous study [31]. Consequently, we examined the influence of pressure, a key parameter in SPS processing, at 1 800 °C, where substantial enhancements in sintered density and hardness were observed.

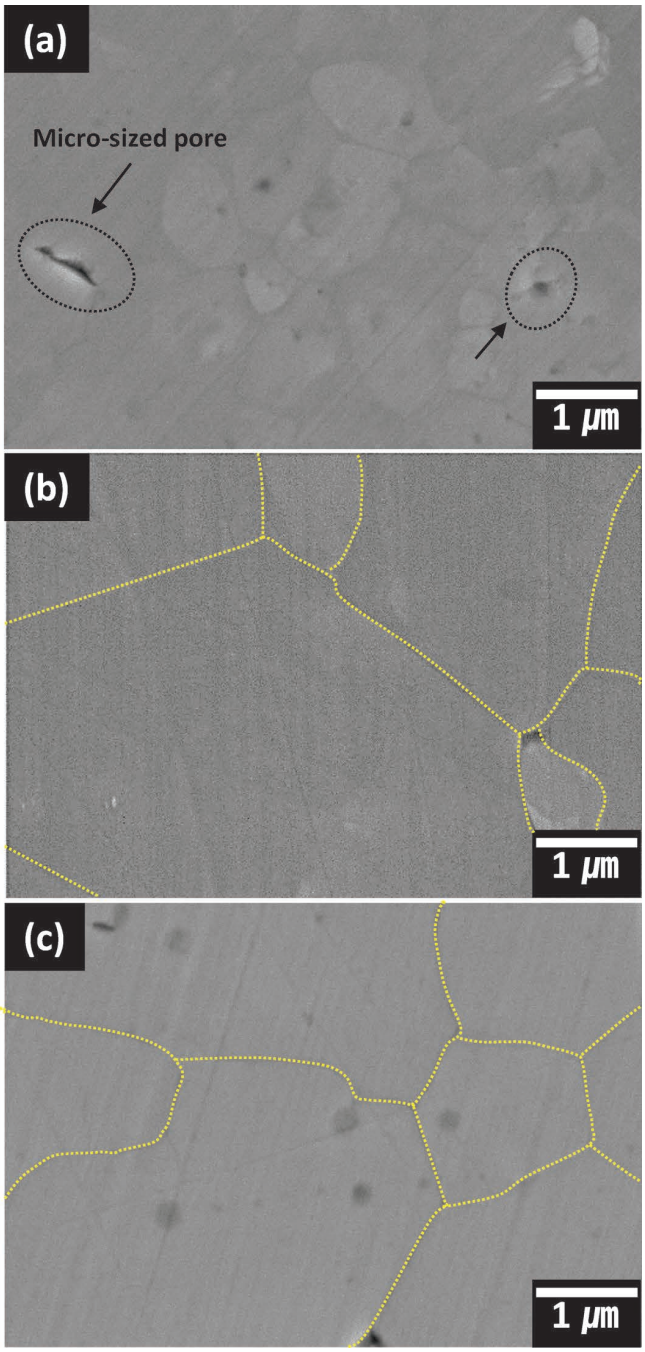

Fig. 4: Cross-sectional FE-SEM micrographs of (Hf-Ta-Ti-Zr-Nb)C high-entropy carbides sintered bulk with different SPS conditions. (a) single-step, 1 800 °C, 20.0 kX, (b) 2 000 °C, 50 MPa, 10 min(single-step), 20.0 kX and (c) 2 000 °C, 60 MPa, 1 min(multi-step), 20.0 kX.

Fig. 6 illustrates the effect of varying pressure on the relative density and Vickers hardness of HEC sintered at 1 800 °C with the single-step SPS technique. As the sintering pressure increases from 50 MPa to 60 MPa, a slight increase in density from 97 % to approximately 97.9 % is observed. Similarly, Vickers hardness rises from 1 770 HV to a maximum of 1 840 HV. These results indicate that the mechanical properties of binder-less carbide can be enhanced at a sintering temperature of 1 800 °C and pressure of 60 MPa. Employing these conditions during the multi-step SPS sintering process may potentially yield even better results at 2 000 °C.

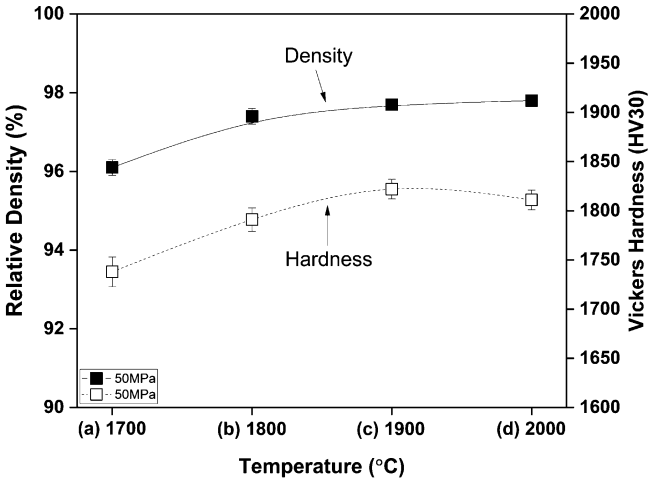

Fig. 5: Relative density and Vickers hardness of (Hf-Ta-Ti-Zr-Nb)C high-entropy carbide sintered bulk as a function of sintering temperatures (a) 1 700 °C, (b) 1 800 °C, (c) 1 900 °C, and (d) 2 000 °C.

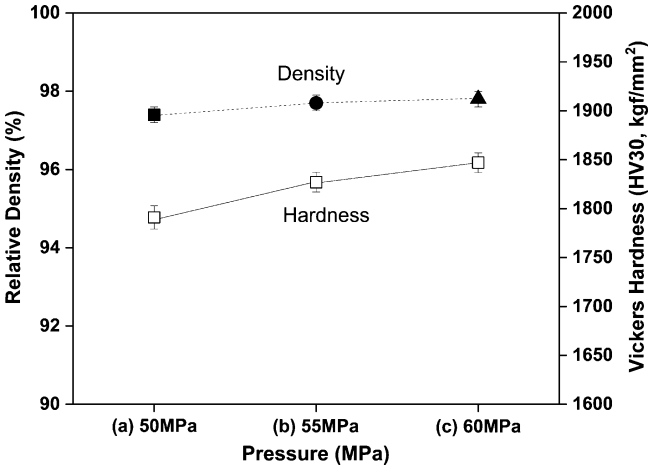

Fig. 6: Relative density and Vickers hardness of (Hf-Ta-Ti-Zr-Nb)C high-entropy carbide sintered bulk as a function of sintering pressures at 1 800 °C (a) 50 MPa, (b) 55 MPa, and (c) 60 MPa.

Fig. 7 describes the impact of single-step and multi-step SPS techniques on the relative density and Vickers hardness of HEC as a function of sintering holding time and pressure variation at 2 000 °C. Multi-step SPS is found to produce higher HEC density (98.1 %) and Vickers hardness (1 910 HV) values compared to single-step SPS. An increase in grain size at 2 000 °C leads to a reduction in Vickers hardness, which is attributed to the consequent decrease in mechanical properties. These results are in agreement with prior microstructural observations, indicating that multi-step sintering is a more effective strategy for achieving maximum HEC densification at a relatively low temperature of 1 800 °C while suppressing grain growth and retaining mechanical properties through a short holding time at the final sintering temperature of 2 000 °C.

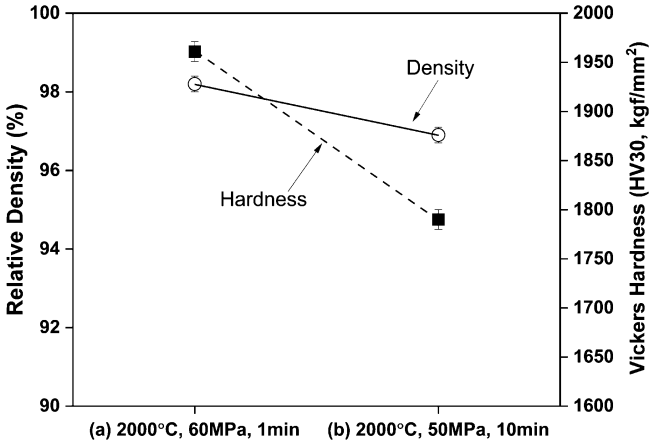

Fig. 7: Relative density and Vickers hardness of (Hf-Ta-Ti-Zr-Nb)C high-entropy carbide sintered bulk as a function of different SPS methods (a) 2 000 °C, 60 MPa, 1 min (multi-step) and (b) 2 000 °C, 50 MPa, 10 min (single-step).

Fig. 8 shows the relative density and Vickers hardness of sintered bulks of high-entropy carbide (HEC) fabricated using single-step and multi-step SPS processes. HEC sintered bulks produced via single-step and multi-step SPS had densities of about 96.9 % and 98.2 %, with hardness of 1 790 HV and 1 960 HV, respectively. A study on the densification of molybdenum powder using spark plasma sintering found that sintering temperature and holding time were the main controlling factors. A relative density of 100 % was achieved at a sintering temperature of 1 850 °C and a holding time of 30 minutes. However, the study also observed a slight decrease in hardness with increasing temperature and time, which could be attributed to an increase in grain size [35]. Therefore, the multi-step SPS process effectively controlled grain growth and enhanced density and hardness.

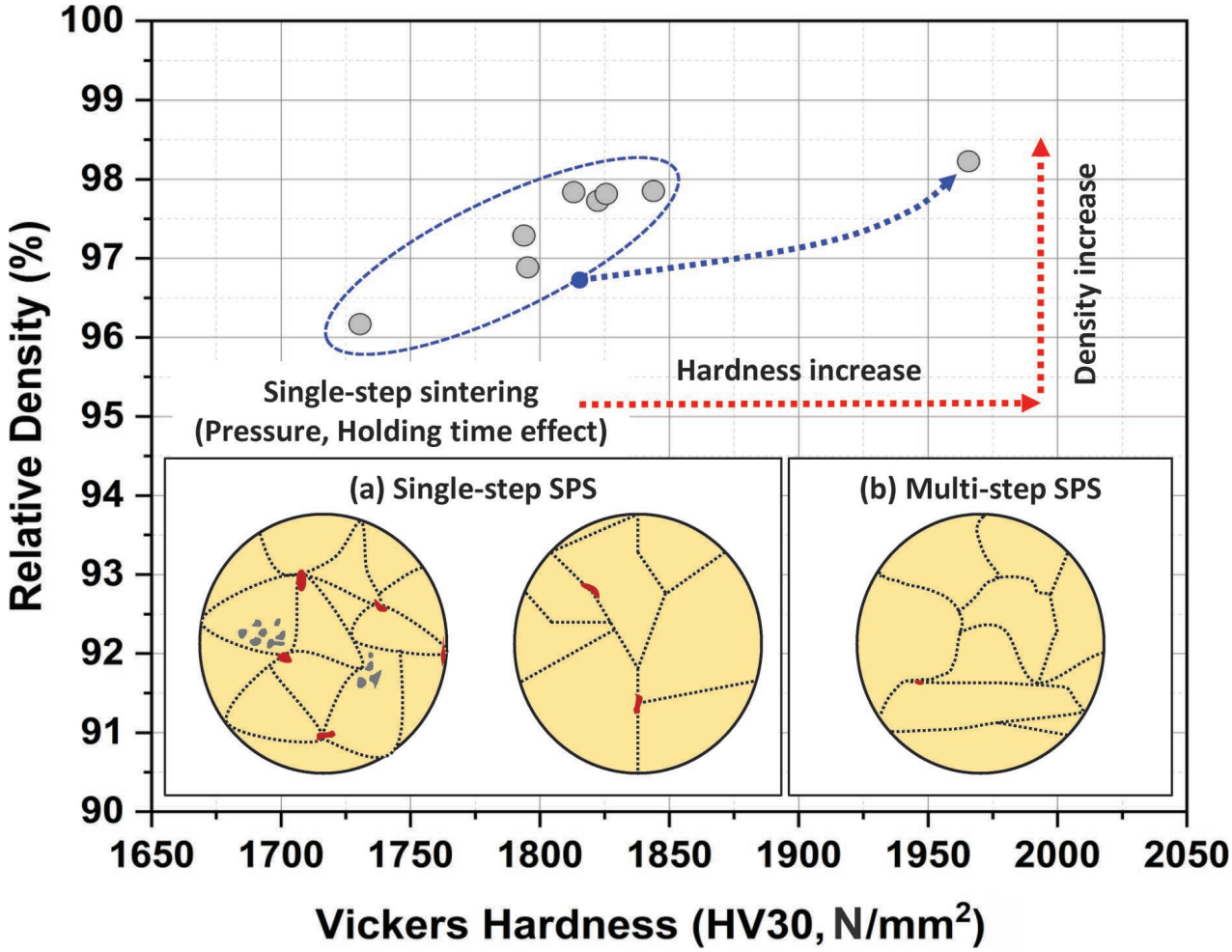

Fig. 8: Comparison of (Hf-Ta-Ti-Zr-Nb)C high-entropy carbide sintered bulk as a function of different SPS methods; Scheme of high-entropy carbide grain size formation during the SPS (a) single-step SPS and (b) multi-step SPS.

IV. Conclusions

In conclusion, this study investigated the fabrication of (Hf-Ta-Ti-Zr-Nb)C high-entropy carbides using a multi-step SPS process to produce dense and homogeneous carbide materials with enhanced mechanical properties. HECs have attracted considerable interest in recent years due to their unique combination of superior mechanical and physical properties, making them ideal for high-temperature applications in aerospace, drilling, and cutting tools for mining and industrial use.

The multi-step SPS process involved the compaction of a high-entropy carbide powder mixture into a green body, followed by sintering under high-temperature plasma generated by a pulsed direct current voltage. This multi-step approach aimed to overcome the limitations of single-step SPS, enabling the production of uniform microstructures with superior material properties.

The results presented here demonstrate that the multi-step SPS process can effectively fabricate high-entropy carbides with high density and hardness, thereby improving the mechanical properties of the final product. Consolidation technology for HEC powders was developed, and the effects of sintering temperature and uniaxial pressure during the SPS process were investigated.

Overall, the multi-step SPS process emerges as a promising technique for the production of advanced high-entropy carbide materials, offering potential for widespread application in various industries requiring materials with exceptional mechanical properties and stability at elevated temperatures.

Acknowledgement

This work was supported by a grant from the National Research Foundation of Korea (NRF) funded by the Korean Government (MSIT) (NRF-2020M3D1A2102213), and the Technology Innovation Program (20017502, Development of the Carbide/PCBN Cutting Tool and the Customized Cutting Solution for High Hardened Steel, by Machine Learning) funded by the Ministry of Trade, Industry & Energy(MOTIE, Korea), and the Korean Institute of Industrial Technology as “Development of root technology for multi-product flexible production” (KITECH EO-23-0008).

References

1 Yeh, J.W., Chen, Y.L., Lin, S.J., Chen, S.K.: High-entropy alloys – a new era of exploitation, *Mater. Sci. Forum.*, **560**, 1 – 9, (2007).

2 Yeh, J.W., Chen, S.K., Lin, S.J., Gan, J.Y., Chin, T.S., Shun, T.T., Tsau, C.H., Chang, S.Y.: Nanostructured high-entropy alloys with multiple principal Elements: novel alloy design concepts and outcomes, *Adv. Eng. Mater.*, **6**, 299 – 303, (2004).

[3] Ji, W., Wang, W., Wang, H., Zhang, J., Wang, Y., Zhang, F., Fu, Z.: Alloying behavior and novel properties of CoCrFeNiMn high-entropy alloy fabricated by mechanical alloying and spark plasma sintering, *Intermetallics*, **56**, 24 – 7, (2015).

[4] Otto, F., Dlouhý, A., Somsen, C., Bei, H., Eggeler, G., George, E.P.: The influences of temperature and microstructure on the tensile properties of a CoCrFeMnNi high-entropy alloy, *Acta Mater.*, **61**, 5743 – 5755, (2013).

[5] Anand, G., Wynn, A.P., Handley, C.M., Freeman, C.L.: Phase stability and distortion in high-entropy oxides, *Acta Mater.*, **146**, 119 – 125, (2018).

[6] Huang, Y.S., Chen, L., Lui, H.W., Cai, M.H., Yeh, J.W.: Microstructure, hardness, resistivity and thermal stability of sputtered oxide films of $AlCoCrCu_{0.5}NiFe$ high-entropy alloy, *Mater. Sci. Eng. A.*, **457**, 77 – 83, (2007).

[7] Wen, L.H., Kou, H.C., Li, J.S., Chang, H., Xue, X.Y., Zhou, L.: Effect of aging temperature on microstructure and properties of AlCoCrCuFeNi high-entropy alloy, *Intermetallics*, **17**, 266 – 269, (2009).

[8] Cantor, B., Chang, I.T.H., Knight, P., Vincent, A.J.B.: Microstructural development in equiatomic multicomponent alloys, *Mater. Sci. Eng., A.*, **375**, 213 – 218, (2004)

[9] Tsai, M.H., Yeh, J.W.: High-entropy Alloys: A critical review, *Mater. Res. Lett.*, **2**, 107 – 123, (2014).

[10] He, J.Y., Wang, H., Huang, H.L., Xu, X.D., Chen, M.W., Wu, Y., Liu, X.J., Nieh, T.G., An, K., Lu, Z.P.: A precipitation-hardened high-entropy alloy with outstanding tensile properties, *Acta Mater.*, **102**, 187 – 196, (2016).

[11] Ye, B., Wen, T., Huang, K., Wang, CZ., Chu, Y.: First-principles study, fabrication, and characterization of $(Hf_{0.2}Zr_{0.2}Ta_{0.2}Nb_{0.2}Ti_{0.2})C$ high-entropy ceramic, *J. Am. Ceram. Soc.*, **102**, 4344 – 4352, (2019).

[12] Dusza, J., Švec, P., Girman, V., Sedlák, R., Castle, E.G., Csanádi, T., Kovalčíková, A., Reece, M.J.: Microstructure of (Hf-Ta-Zr-Nb)C high-entropy carbide at micro and nano/atomic level, *J. Eur. Ceram. Soc.*, **38**, 4303 – 4307, (2018).

[13] Zhang, R.Z., Reece, M.J.: Review of high entropy Ceramics: design, synthesis, structure and properties, *J. Mater. Chem. A.*, **7**, 22148 – 22162, (2019).

[14] Yang, Y., Wang, W., Gan, G.Y., Shi, X.F., Tang, B.Y.: Structural, mechanical and electronic properties of (TaNbHfTiZr)C high entropy carbide under Pressure: ab initio investigation, *Physica B.*, **550**, 163 – 170, (2018).

[15] Harrington, T.J., Gild, J., Sarker, P., Toher, C., Rost, C.M., Dippo, O.F., McElfresh, C., Kaufmann, K., Marin, E., Borowski, L., Hopkins, P.E., Luo, J., Curtarolo, S., Brenner, D.W., Vecchio, K.S.: Phase stability and mechanical properties of novel high entropy transition metal carbides, *Acta Mater.*, **166**, 271 – 280, (2019).

[16] Zhang, H., Akhtar, F.: Processing and characterization of refractory quaternary and quinary high-entropy carbide composite, *Entropy*, **21**, 474, (2019).

[17] Peng, C., Gao, X., Wang, M., Wu, L., Tang, H., Li, X., Zhang, Q., Ren, Y., Zhang, F., Wang, Y.: Diffusion-controlled alloying of single-phase multi-principal transition metal carbides with high toughness and low thermal diffusivity, *Appl. Phys. Lett.*, **114**, 011905, (2019).

[18] Ye, B., Wen, T., Liu, D., Chu, Y.: Oxidation behavior of $(Hf_{0.2}Zr_{0.2}Ta_{0.2}Nb0.\ 2Ti_{0.2})C$ high-entropy ceramics at 1073 – 1473 K in air, *Corros. Sci.*, **153**, 327 – 332, (2019).

[19] Wang, H., Cao, Y., Liu, W., Wang, Y.: Oxidation behavior of $(Hf_{0.2}Ta_{0.2}Zr_{0.2}Ti_{0.2}Nb_{0.2})C$-xSiC ceramics at high temperature, *Ceram. Int.*, **46**, 11160 – 11168, (2020).

[20] Yan, X., Constantin, L., Lu, Y., Silvain, J.F., Nastasi, M., Cui, B.: $(Hf_{0.2}Zr_{0.2}Ta_{0.2}Nb_{0.2}Ti_{0.2})C$ high-entropy ceramics with low thermal conductivity, *J. Am. Ceram. Soc.*, **101**, 4486 – 4491, (2018).

[21] Zhang, Q., Zhang, J., Li, N., Chen, W.: Understanding the electronic structure, mechanical properties, and thermodynamic stability of (TiZrHfNbTa)C combined experiments and first-principles simulation, *J. Appl. Phys.*, **126**, 025101, (2019).

[22] Chen, Y., Wang, J., Chen, M.: Enhancing the machining performance by cutting tool surface modifications: A focused review, *Mach. Sci. Technol.*, **23**, 477 – 509, (2019).

[23] Harrington, T.J.: High entropy carbides: modeling, synthesis, and properties, UC San Diego, (2019).

[24] Oses, C., Toher, C., Curtarolo, S.: High-entropy ceramics, *Nat. Rev. Mater.*, **5**, 295 – 309, (2020).

[25] Feng, L., Fahrenholtz, W.G., Hilmas, G.E.: Low-temperature sintering of single-phase, high-entropy carbide ceramics, *J. Am. Ceram. Soc.*, **102**, 7217 – 7224, (2019).

[26] Zhang, H.: High-entropy boron-carbide and its composites, Luleå University of Technology, (2020).

[27] Sarker, P., Harrington, T., Toher, C., Oses, C., Samiee, M., Maria, J.P., Brenner, D.W., Vecchio, K.S., Curtarolo, S.: High-entropy high-hardness metal carbides discovered by entropy descriptors, *Nat. Commun.*, **9**, 4980, (2018).

[28] Castle, E., Csanádi, T., Grasso, S., Dusza, J., Reece, M.: Processing and properties of high-entropy ultra-high temperature carbides, *Sci. Rep.*, **8**, 8609, (2018).

[29] Zhou, J., Zhang, J., Zhang, F., Niu, B., Lei, L., Wang, W.: High-entropy Carbide: A novel class of multicomponent ceramics, *Ceram. Int.*, **44**, 22014 – 22018, (2018).

[30] Wei, X.F., Liu, J.X., Li, F., Qin, Y., Liang, Y.C., Zhang, G.J.: High entropy carbide ceramics from different starting materials, *J. Eur. Ceram. Soc.*, **39**, 2989 – 2994, (2019).

[31] Song, J., Duong, L.V., Trinh, P.V., Linh, N.N., Phuong, D.D., Seok, J., Kim, S.Y., Han, J., Kim, H.: Characteristics and sintering behavior of (Hf-Ta-Ti-Zr-Nb)C high-entropy carbides fabricated by high-energy ball milling and spark plasma sintering, *J. Ceram. Sci. Technol.*, 1 – 8, (2022).

[32] Pötschke, J., Dahal, M., Herrmann, M., Vornberger, A., Matthey, B., Michaelis, A.: Preparation of high-entropy carbides by different sintering techniques, *J. Mater. Sci.*, **56**, 11237 – 11247, (2021).

[33] Moskovskikh, D.O., Vorotilo, S., Sedegov, A.S., Kuskov, K.V., Bardasova, K.V., Kiryukhantsev-korneev, Ph.V., Zhukovskyi, M., Mukasyan, A.S.: High-entropy (HfTaTiNbZr)C and (HfTaTiNbMo)C carbides fabricated through reactive high-energy ball milling and spark plasma sintering, *Ceram. Int.*, **46**, 19008 – 19014, (2020).

[34] Chaim, R, Chevallier, G., Weibel, A., Estournès, C.: Grain growth during spark plasma and flash sintering of ceramic nanoparticles: A review, *J. Mater. Sci.*, **53**, 3087 – 3105, (2017).

[35] Mouawad, B., Soueidan, M., Fabrègue, D., Buttay, C., Bley, V., Allard, B., Morel, H.: Full densification of molybdenum powders using spark plasma sintering, *Metall. Mater. Trans. A Phys. Metall. Mater. Sci.*, **43**, 3402 – 3409, (2012).